In-depth characterization of the Syrian hamster as translational model for COVID-19 in humans

Martina Castellan[1,2]†, Gianpiero Zamperin[1,3]†, Giulia Franzoni[4], Greta Foiani[5], Maira Zorzan[1,2], Petra Drzewnioková[1,2], Marzia Mancin[6], Irene Brian[1,7], Alessio Bortolami[1,8], Matteo Pagliari[1,8], Annalisa Oggiano[4], Marta Vascellari[5], Valentina Panzarin[1,7], Sergio Crovella[9], Isabella Monne[1,3], Calogero Terregino[1], Paola De Benedictis[1,2] and Stefania Leopardi[1,2*]

[1] Division of Comparative Biomedical Sciences, Istituto Zooprofilattico Sperimentale delle Venezie, Legnaro, Italy
[2] Laboratory for Emerging Viral Zoonosis, Istituto Zooprofilattico Sperimentale delle Venezie, Legnaro, Italy
[3] Laboratory for Viral Genomics and Trascriptomics, Istituto Zooprofilattico Sperimentale delle Venezie, Legnaro, Italy
[4] Laboratory of Diagnostic Virology, Istituto Zooprofilattico Sperimentale della Sardegna
[5] Laboratory of Histopathology, Istituto Zooprofilattico Sperimentale delle Venezie, Legnaro, Italy
[6] Risk Analysis and Public Health Department, Istituto Zooprofilattico Sperimentale delle Venezie, Legnaro, Italy
[7] Innovative Virology Laboratory, Istituto Zooprofilattico Sperimentale delle Venezie, Legnaro, Italy
[8] Laboratory of Experimental Animal Models, Istituto Zooprofilattico Sperimentale delle Venezie, Legnaro, Italy
[9] Biological Science Program, Department of Biological and Environmental Sciences, College of Arts and Sciences, Qatar University, Doha
† These authors contributed equally to this work
* Correspondence and requests for materials should be addressed to S.L. (sleopardi@izsvenezie.it)

The recent emergence of severe acute respiratory syndrome coronavirus 2 (SARS-CoV-2) has highlighted the importance of having proper tools and models to study the pathophysiology of emerging infectious diseases to test therapeutic protocols, assess changes in viral phenotype and evaluate the effect of viral evolution. This study provides a comprehensive characterization of the Syrian hamster (*Mesocricetus auratus*) as an animal model for SARS-CoV-2 infection, using different approaches (description of clinical signs, viral replication, receptor profiling and host immune response) and targeting four different organs (lungs, intestine, brain and PBMCs). Our data showed that both male and female hamsters are susceptible to the infection and develop a disease similar to the one observed in patients with COVID-19, including moderate to severe pulmonary lesions, inflammation and recruitment of the immune system in lungs and at systemic level. However, all animals recovered within 14 days without developing the severe pathology seen in humans, and none of them died. We found faint evidence for intestinal and neurological tropism associated with absence of lesions and a minimal host response in intestines and brains, highlighting another crucial difference with the multi-organ impairment of severe COVID-19. When comparing male and female hamsters, it was observed that males sustained higher viral shedding and replication in lungs, suffered from more severe symptoms and histopathological lesions and triggered higher pulmonary inflammation. Overall, these data confirm the Syrian hamster as being a suitable model for mild-moderate COVID-19 and reflect sex-related differences in the response against the virus observed in humans.

Introduction

The pandemic of coronavirus disease 2019 (COVID-19) has resulted in a devastating global threat to human society, economy and healthcare system[1–3]. The disease is caused by severe acute respiratory syndrome coronavirus 2 (SARS-CoV-2), a positive-sense single-stranded RNA virus belonging to the subgenus *Sarbecovirus,* genus *Betacoronavirus*, species *SARS-related coronavirus,* likely emerged from animals after zoonotic cross-species transmission[4,5]. The virus mostly replicates in the respiratory tract, but patients may also experience disorders associated to multi-organ engagement, including neurologic and gastro enteric symptoms, whose incidence, mechanism and significance is still a matter of discussion[6–10]. According to the age of the patient and the presence of predisposing factors, COVID-19 varies widely in the severity of its clinical manifestations, spanning from asymptomatic infections to an acute respiratory distress syndrome (ARDS) requiring mechanical ventilation and, in the worst-case scenario, to death[11–13]. Epidemiological data indicate that males are more prone to develop a severe COVID-19 symptomatology[14–16], suggesting that sex may also influence SARS-CoV-2 pathogenesis due to genetic and hormonal factors, although social-behavioral differences between genders may also play a role[14]. Regardless of the cause, the development of severe disease follows a common mechanism in the dysregulation of the inflammatory response, similarly to what has been observed with other coronavirus infections, such as Severe Acute Respiratory Syndrome (SARS) and Middle East Respiratory Syndrome (MERS)[11]. Briefly, in the attempt to clear the infection, the immune system of certain individuals releases an excessive amount of pro-inflammatory cytokines, known as "cytokine storm", promoting an uncontrolled inflammation that damages lungs and other organs, such as brain, gut and heart[17,18]. This important evidence has paved the way for a diagnostic, prognostic and therapeutic approach focused on controlling patients' immune response, with particular attention to the innate immunity[19,20]. The overarching goal is to control the pandemic by reducing the incidence of severe manifestations through vaccination campaigns, and to develop and assess the efficacy of therapeutic agents against the new variants deriving from the evolution of SARS-CoV-2. Among them, the WHO classifies as "variants of concern (VOCs)" viruses[21] that show mutations on the spike protein that might influence transmissibility, symptomatology, immune-protection, efficacy of therapeutic monoclonal antibodies and sensitivity of diagnostic methods[22–29]. In this race, researchers need reliable animal models that i) are susceptible to the infection, ii) are able to eliminate the virus, iii) display clinical and pathological manifestations typical of human disease, and iv) mimic the same immune disorder found in patients. Non-human primates, ferrets, hamsters, and transgenic mice (i.e. K18-hACE2 mouse) are permissive to SARS-CoV-2 infection and develop lung lesions resembling pathological patterns found in humans[30–34]. Among these, the Syrian hamster (*Mesocricetus auratus*) exhibits the best balance between costs, neurological development, easy handling and maintenance in captivity and it is extensively used for translational medicine[32,35,36]. Previous studies showed that SARS-CoV-2 replicates efficiently in the respiratory tract of hamsters and is able to invade the central nervous system, with no differences observed between animals of different age[35]. Histopathological and radiographic evaluations confirmed that these animals develop severe pneumonia without showing severe clinical manifestations and fully recover in 2-3 weeks[35,37]. In addition, preliminary studies showed that hamsters increase the gene expression of some cytokines/chemokines in the lungs, which may be compatible with the cytokine storm described in humans[38]. The aim of this study is to provide an in-depth evaluation of the Syrian hamster as animal model for human COVID-19, and to identify the advantages and disadvantages of using this species for translational medicine. Our work provides new outcomes to take into account while

designing an infection study using this animal model, including evidence for sex-related differences.

Results

Infection and seroconversion. Syrian hamsters intranasally infected with the B.1.1.7 SARS-CoV-2 VOC developed no clinical signs, except for a 5% drop in body weight between 2 and 6 days post infection (dpi), with subsequent recovery (Fig. 1a; Supplementary Table 1). Viral shedding started at 2 dpi, peaked between 4 and 6 dpi depending on the sex and dropped shortly after. Virus genome was detectable until 14 dpi with high CT values; males showed higher shedding across the whole study period (P<0.0001, Fig. 1b) with a mean delta of 3.6 CT (Fig. 1b; Supplementary Table 1).
All infected individuals produced detectable neutralizing antibodies against SARS-CoV-2 from 6 dpi, reaching the highest titers 14 dpi (Fig. 1c). Geometric mean titers (GMT) were higher in males rather than females, but the difference was not statistically significant.
SARS-CoV-2 established a productive infection in the lungs, with viral RNA detected in all individuals with decreasing viral load over time (Fig. 1d). We confirmed these results by showing the presence of the spike protein in the pulmonary parenchyma of all individual using immunofluorescence. Interestingly, the lungs of male hamsters collected 6 dpi also showed a marked expression of double-strand RNA (dsRNA), which is an indicator of active viral replication, whereas only a weak signal could be observed in the lungs of the females at the same time point (Fig. 1e). Mock animals did not stain for any of the tested antibodies, confirming the specificity of reactions. Evidence for SARS-CoV-2 infection in the intestines and brains was far less marked, with low viral load and inconsistent results within the infected groups. On day 14, only one individuals was positive for each group in both organs (Fig. 1d). Coherently with these results, immunofluorescence staining for viral spike glycoprotein and ds-RNA was evident only in the intestinal sections of two males at 2 dpi (Supplementary Fig. 1a).

Pathology. Lungs of male hamsters were diffusely consolidated with dark-red coloration at day 6, while multiple dark-red consolidated areas were scattered throughout all lobes of females. At 14 dpi, we observed few small reddish foci independently of the sex.
Histopathogical changes in the lungs were consistent with a bronchointerstitial pneumonia (Fig. 2a-c), with cumulative histopathological score peaking on day 6 in both sexes (Fig. 2d; Supplementary Table 2). At 2 dpi, main histopathological changes consisted in mild-to-moderate alveolar damage, with alveolar activated macrophages, few neutrophils and vascular hyperemia (Fig. 2a). At 6 dpi, extensive and coalescing inflammatory foci with parenchymal consolidation affected more than 75% of the surface in 3 individuals, 50-75% in 5, and 25-50% in 2 females. In all animals, alveolar damage was associated with intense pneumocyte type II and bronchiolar epithelium hyperplasia (Fig. 2b and Fig. 2g.1). We detected scattered syncytial multinucleated cells in bronchioles and alveolar surfaces that, in one case, contained 2-4 µm amphophilic round cytoplasmic inclusions consistent with viral-like particles (Fig. 2g.2). At this stage, edema and infiltration of inflammatory cells (perivascular lymphomonocytic cuffs, alveolar macrophages and neutrophils) were moderate-to-severe, slightly more abundant in males (Fig. 2e, f and Supplementary Table 2). Pre- and post-capillary vasculature exhibited plumped reactive endothelium with sub-endothelial infiltration of lymphocytes, monocytes and rare neutrophils in most animals, consistent with endothelialitis[39] (Fig. 2g.3). The infiltration of inflammatory cells decreased by day 14 when only few lymphocytes, plasma cells and histiocytes surrounding the alveolar ducts were observed. Alveoli adjacent to terminal/respiratory bronchioles were multifocally lined by cells resembling bronchiolar epithelium (alveolar bronchiolization)[40,41] (Fig. 2g.4). There was no evidence of fibroplasia and reparative fibrosis (Fig. 2c).

Intestines and brains showed no gross nor histologically detectable lesions (Supplementary Fig. 1b-c).

Host response to SARS-CoV-2 infection. To study male and female host response against SARS-CoV-2, we performed an RNA-Seq analysis on lungs, intestines, brains and peripheral blood mononuclear cells (PBMCs) at three different time points. The comparison of the expression profile of all tissues from infected and mock individuals of the same sex and time point allowed us to quantify and describe the host response in terms of differentially expressed genes (DEGs) (Supplementary Table 3-4). In the lungs, response began at 2 dpi, reached the apex at 6 dpi and was still persistent in the latest time point, with no substantial differences between male and female hamsters. Females PBMCs exhibited the same parabolic curve observed in the lungs, while males elicited a stronger systemic response involving more than 2000 DEGs throughout the study (Fig. 3a-b and Supplementary Table 3-4). In intestines and brains, consistently with viral presence and replication, we observed that host response was far less marked. In both organs, females and males followed opposite trends, with DEGs number increasing in females and decreasing in males (Fig. 3b). We then employed Gene Ontology (GO) resource to investigate biological processes enriched in SARS-CoV-2-infected Syrian hamsters (Supplementary Table 5). Except for the intestines of males that showed many enriched GO terms, the number of enriched processes followed the same trend of DEGs in all tissues and sexes (Fig. 3c).

To better investigate how Syrian hamster respond to SARS-CoV-2, we focused on GO terms associated to the immune response and correlated biological functions. In the lungs, some GO terms showed the same pattern of enrichment across sexes, being activated in all the infected hamsters at 2 dpi (e.g. “cellular response to type I interferon”), 6 dpi (e.g. “T cell receptor signaling pathway” and “response to interferon-gamma”) or both (e.g. “inflammatory response”, “defense response to virus”, “activation of immune response”, “cytokine-mediated signaling pathway”) (Fig. 4a). On the other hand, at 6 dpi some GO terms were exclusively enriched in males (e.g. “angiogenesis” and “negative regulation of immune system process”) or exclusively in females (“regulation of B cell differentiation”) (Fig. 4a).

In both intestines and brains, we did not find a clear inflammatory pattern in response to the infection with SARS-CoV-2.

In the intestines we found few GO terms related to the immune system. At 2 dpi, “positive regulation of innate immune response”, “defense response to virus” and “cellular response to interferon-alpha”, were enriched in both sexes, while “cellular response to interferon-beta” and “toll-like receptor signaling pathway” were specifically enhanced in males. Only three GO terms of very general means (e.g. “inflammatory response”) were enriched at 6 dpi, while at 14 dpi we detected GO terms related to lesions recovery, such as “wound healing”, and “tissue regeneration”. At this time point, we noted few sex-specific enriched terms, such as “positive regulation of T cell differentiation”, “lymphocyte differentiation” and “B cell activation” in males and “antigen receptor-mediated signaling pathway”, “chemokine-mediated and cytokine-mediated signaling pathways” in females.

In the brains, few GO terms were enriched in both sexes exclusively 2 dpi, including “activation of immune response”, “complement activation”, “defense response to virus”, “cellular response to interferon-alpha and -beta” (Fig. 4c).

As a major novelty of this study, we analyzed the immunological profile of PBMCs to investigate the Syrian hamster systemic activation of the immune system, searching for potential similarities with human severe COVID-19 cases. We observed the activation of the immune response in both sexes in all the three time points, as expressed by longitudinal enrichment of related GO terms such as “cytokine/chemokine-mediated signaling pathway”, “regulation of lymphocyte activation”, “inflammatory response”, “programmed cell death”

and "defense response to virus" (Fig. 5a). Other GO terms enriched in both sexes during the experiment at any time point, included "complement activation", "antigen processing and presentation of peptide antigen via MHC class I", "positive regulation of innate immune response" and "toll-like/pattern recognition receptor signaling pathway". Some GO terms were enriched in a sex-specific manner, such as "regulation of autophagy" and "lymphocyte differentiation in males", or "cellular response to interferon-alpha" and, "alpha-beta T cell activation" in females. In particular, we observed major differences between females and males at 14 dpi, when 98% of the up-regulated genes (2676/2723) were male-specific and 60% of down-regulated genes (401/672) were female-specific (Fig. 5b and Supplementary Table 4).

Syrian Hamster as immunological model for COVID-19. To investigate whether hamsters display the typical immunological profiles described in COVID-19 lungs, we evaluated the expression levels of 100 genes associated to a severe human condition (Fig. 6a). Syrian hamsters activated an Interferon-I (IFN-I)-mediated cell-specific response to the virus at 2 dpi, as shown by the up-regulation of many interferon stimulated genes (ISGs). This included genes coding for IFIT proteins (e.g. *Ifit2*, *Ifit3*), members of the OAS family (e.g. *Oas1*, *Oas2*, *Oas3*, *Oasl*), interferon regulatory factors (e.g. *Irf7* and *Irf9*) and several genes involved with cellular mechanisms of antiviral response (e.g. *Ddx60*, *Parp12* and *Parp14*). Specific immune response increased in both sexes at 6 dpi, with upregulation of 58 and 50 out of 100 target genes for males and females respectively. SARS-CoV-2- infected animals promoted immune cell recruitment with complement activation, immunoglobulin-mediated response, and strong upregulation of pro-inflammatory cytokines (e.g. *Ccl2*, *Ccl3*, *Cxcl10*, *Il6* and *Ifnγ*) moreover, we observed activation of genes involved in monocyte (*Cd33*, *Cd16* and *Siglec1*) and T-cell activation (*Tbx21*, *Cd40lg*, *Cd4*, *Cd8a* and *Cd8b*). At 6 dpi males also up-regulated genes associated with active neutrophils recruitment (e.g. *Mmp9*, *Cd11c*, *Fut4* and *Elane*) and angiogenesis (e.g. *Mmp3*, *Thbs1* and *Angptl4*) (Fig. 6a). Interestingly, male hamsters downregulated both SARS-CoV-2 receptor *Ace2* and its receptor *Agtr1* genes. Of note, immunofluorescence staining for ACE2 expression confirms the sex-specific reduction of the receptor in lung tissue compared to mock controls (Fig. 6b). Hamsters of both sexes shut down almost completely the specific pulmonary immune response by day 14, with no individual perpetuating the immune exasperation and inflammation typical of severe COVID-19.

Among 32 key immunological genes associated to a severe COVID-19 systemic pathology in humans, 24 were differentially expressed in hamsters' PBMCs in at least one case (Fig. 6c). Our results present a male-biased up-regulation of genes associated with immature neutrophils activation (e.g. *Cd49d*, *Cd274*, *Tlr4* and *Cd43*) and pro-inflammatory cytokines associated with the cytokine storm (*Il1β*, *Il6* and *Tnf*). In this context, the longitudinal monitoring of pro-inflammatory IL-1β and IL-6 revealed their low release in the serum in response to SARS-CoV-2 infection, with exclusive increase in circulating levels of IL-1β in male hamsters at 14 dpi (Fig. 6d; Supplementary Fig. 2).

Discussion

Following the declaration of the COVID-19 pandemic by WHO in March 2020, both the scientific community and health authorities were on the frontline for the development of control measures to limit the spread of the infection and mitigate disease severity. To achieve this goal translational animal models were used to elucidate the pathogenesis of the disease and to rapidly assess the efficacy of prophylactic and therapeutic agents. However, in order for scientists to select the best animal model for their studies, it is crucial to characterize in which way a species can mimic the host-pathogen relationship between humans and SARS-CoV-2. In this study, we provide a comprehensive description for the Syrian hamsters that, also before the emergence of SARS-CoV-2, was an animal model used extensively to study other zoonotic emerging diseases, including bunyaviruses, arenaviruses, henipaviruses, flaviviruses, alphaviruses, filoviruses, as well as the coronaviruses SARS-CoV and MERS-CoV[42]. We performed experimental infections using SARS-CoV2 B.1.1.7 strain or Alpha VOC, isolated in Italy. The Alpha VOC was first detected in November 2020 in the United Kingdom and rapidly spread all across Europe, being responsible for increased of infections during the second epidemic wave. Compared to older strains, this variant was associated with higher transmissibility and, according to some studies, increased mortality rates. In Italy, it was the most prevalent variant between February and March 2021 [43,44].In our study, we successfully infected all the hamsters, detecting SARS-CoV-2 in tissues and oropharyngeal swabs from day 2 to 14 and specific antibody response by day 6, supporting earlier evidences[35,45]. In addition, we confirmed the presence of the antigen within pulmonary tissue up to 14 dpi through immunofluorescence, using a specific antibody directed towards the spike protein. On the other hand, the use of another antibody that is generally directed towards dsRNA, showed positive staining only in male lungs at 6 dpi. As dsRNA is a replicative intermediate of many RNA viruses, coronaviruses included [46,47], this result indicates a higher replication rate in males at 6 dpi, even if it did not translate into an evident increase in the molecular detection of the virus using ddPCR. In this sense, paired immunofluorescence and molecular investigations performed at intermediate timepoints might have helped elucidating the dynamics of viral infection and replication within the pulmonary tissue of female and male hamsters.

SARS-CoV-2-infected hamsters developed a moderate-to-severe bronchointerstitial pneumonia mimicking histological patterns observed in COVID-19 patients (i.e. diffuse alveolar damage, interstitial and intra-alveolar influx of macrophages/neutrophils and pulmonary vascular endothelialitis), as previously described[35,38,45,48]. Alveolar damage is milder, unevenly distributed, with no formation of hyaline membranes typical of human COVID-19[33,49–51].

Despite lung damage, hamsters showed no clinical signs but a significant loss in body weight that resolved spontaneously by day 14 post-infection. This result is consistent with previous reports, although few studies also reported symptoms as lethargy, ruffled fur, hunched back posture and rapid breathing[45], a difference that might be related with the virus (i.e. titer and route of inoculum or viral strain)[35,52], the hamsters (i.e. age)[35,53] or a combination of both[35]. While it is known that prey species such as hamsters mask their sickness in presence of a perceived threat such as humans[54], these data suggest that disease in hamsters mostly resembles that found in humans with mild COVID-19 symptoms. In humans, severe COVID-19 is associated with tissue damage due to an exacerbated inflammatory response[18] and multi-organ failure as secondary effect of systemic activation and exhaustion of the immune system[55,56], or due to viral spread outside the respiratory system[57,58]. In our study, we investigated viral spread and hamsters' immune response at local and systemic level, in order

to evaluate the differences between our animal model and severe cases of COVID-19 in humans.

Hamsters mostly responded to SARS-CoV-2 in the lungs within the first week, with subsequent silencing by the end of the experiment that paired the recovery from the clinical disease, the clearance of the infection and the repair of pathological lesions. Most DEGs and GOs were associated to the immune response and related biological functions, including the activation of IFN-I alpha and beta, which was previously described by Hoagland and colleagues[38]. These molecules are crucial for effective antiviral response because they counteract viral replication in infected cells and cell-to-cell spread, enhance antigen presentation, and promote the development of the adaptive immune response[59,60]. Despite the induction of interferons is dampened after infection with SARS-CoV-2 compared to other viruses such as Influenza A[13,61], IFN-I signalling influences the severity of COVID-19 in humans. Alterations in TLR3-dependent and TLR7-dependent type I interferon induction, the presence of autoantibodies to interferon and, in general, the reduced induction of local and systemic interferon responses against SARS-CoV-2 infection lead to severe manifestations[13]. Indeed, restricted IFN-I response might promote longstanding active viral replication, excessive production of pro-inflammatory cytokines and influx of neutrophils and monocytes, which act as further sources for pro-inflammatory mediators and promote greater tissue damage[18]. In this context, it is likely that the early and powerful induction of IFN-I related genes that we described in hamsters promotes fast viral clearance in the lungs and tissue structure restoration, and prevents severe manifestations of the disease in this animal model. Our data show that, similar to humans, also hamsters respond to the infection with local inflammation, recruitment of immune cells, activation of the complement and immunoglobulin-mediated response, and release of pro-inflammatory cytokines. However, such a response is contained in this animal model and shut down by day 14 post-infection. Furthermore, PBMCs RNA-Seq data showed a modest systemic response in hamsters that resolves within two weeks, with activation of the interferon pathway, innate cell recruitment and activation of lymphocytes B and T and immunoglobulin−mediated immune response. Modest increase in circulating levels of the pro-inflammatory cytokines further corroborates previous studies[62,63] and highlights another crucial difference with patients suffering from complicated COVID-19 that present almost 3-fold higher levels of pro-inflammatory cytokine IL-6 compared to patients with an uncomplicated form of the disease[64]. Overall, our data suggest that hamsters do not suffer of any dysregulation of the immune system that might determine severe COVID-19 in humans.

Consistently with the low systemic activation of the immune system that in humans promotes tissue damage in peripheral districts, we discovered that there were no histopathological lesions in the intestines and brains of the hamsters. In addition, our ddRT-PCR data support other studies in showing limited spread of SARS-CoV-2 outside the respiratory tract in this species[35]. The lower or absent systemic infection in hamsters compared to humans, where the virus can spread to the digestive tract, the brain, the heart, the kidneys, the sweat glands of the skin and the testicles[57,58] further explains the fewer complications seen in this model. Interestingly, we found positive staining in immunofluorescence for the spike and dsRNA supporting replication of the virus in the intestines, with transcriptomic analyses showing weak and generic immune response. While the lack of studies on the transcriptome of human intestines during COVID-19 prevents us from making significant comparisons with our animal model, infection of human small intestinal organoids resulted in much higher transcriptomic signal[65]. On the other hand, the minimal alterations shown in our analyses could simply result from enterocytes sloughing following fasting and weight loss.

In our study, all data supported that infection with SARS-COV-2 has more severe consequences in male hamsters. Indeed, males developed more diffuse and severe lung

lesions, characterized by higher scores of infiltration of inflammatory cells and edema, which may have resulted in the more obvious pathological manifestations. Thanks to the combination of several approaches, our study allowed us to investigate the possible causes and consequences of such a difference. Of note, we found in lungs, males display a higher differential expression of genes associated with activated neutrophils and alveolar macrophages and with the release of pro-inflammatory cytokines associated to ARDS, such as *Il-6*, *Cxcl10* and *Ifn*. This sex-based difference has been evidenced in human COVID-19 cases[66–69] but it had not been previously reported for animal models, where the transcriptome of infected hamsters was mainly investigated using RT-qPCR rather than RNA-Seq analysis[53,70,71]. Another peculiarity of male hamsters standing out from our data is the differential expression of genes promoting angiogenesis (e.g. *Mmp3*, *Thbs1* and *Angptl4*), that might explain sex-driven differences in the pulmonary lesions. Finally, male hamsters downregulate both *Ace2* and its receptor *Agtr1* at day 6, a feature that we were able to identify using transcriptomic analyses and to confirm through immunofluorescence, showing a decreased level of the receptor within pulmonary tissue between non-infected and infected animals. As the receptor gets endocytosed together with the virus during cellular infection, it is possible that this difference is due to a higher level of infection and replication of SARS-CoV-2 in males. Consistently with this hypothesis, we observed a high viral load by ddRT-PCR and a peculiar staining for dsRNA in the lungs of male hamsters. Other than being SARS-CoV-2 cellular receptor, ACE2 has the physiological function of inactivating angiotensin II (AII) molecules produced by ACE, known for its vasoconstrictive activities and, crucially, for acting as a potent pro-inflammatory cytokine[18]. As a further notice, increased level of AII can also exacerbate IL-6 signaling. In this context, several cytokine storm cytokines[55,72] as *Il-6, Il-1* and *Tnf* and genes associated with immature neutrophils activation (e.g. *Itga4*, *Cd274* and *Spn*) were specifically up-regulated in PBMCs from male hamsters only. Similarly, males showed a peculiar increase in serum levels of IL-1β at 14 dpi that was not observed in females, thus suggesting a possible re-acerbation of the systemic inflammation.

These evidences further corroborate a sex-mediated difference in the pathology of COVID-19 in hamsters that could provide useful insights to understand similar evidences in humans.

Indeed, studies worldwide support that more men than women require intensive care or succumb to the disease[15]. While it has been suggested that social and behavioral differences between genders might influence the progression of COVID-19, our data support the role of the biological sex. Finally, the longitudinal assessment of oropharyngeal swabs showed that, while showing akin kinetics, males eliminate more virus, suggesting sex-driven differences also in the epidemiology of the pandemic.

In conclusion, our study provides a comprehensive evaluation of the Syrian hamster as animal model for COVID-19. Overall, we confirmed that the infection with SARS-CoV-2 shows similar pathways in humans and hamsters, which proved to be an excellent model to test the efficacy of prophylactic biologicals, such as vaccines, and to quickly assess the phenotypic changes of new VOCs. However, our study underlines that hamsters only mimic mild-to-moderate COVID-19 and do not replicate the exacerbation of the immune response, which is the cause of severe human cases. In this context, hamsters should be used with caution to evaluate therapeutic agents dampening the immune response. As a final note, we were able to observe a significant difference between female and male hamsters that should be taken into account when designing any experimental study. While this feature is likely not peculiar to the SARS-CoV-2 infection, the sex-biases of animal experiments has long represented a critical aspect of translational medicine[73]. Fortunately, researchers, funders and policy makers unanimously acknowledge the need for a change; research projects that include both sexes and analyses of data by gender – as in the present study - are becoming more and

more popular. In turn, we believe that animal models will progressively become important not only to describe disease pathological pathways but also to grasp differences related to biological sex.

Materials and Methods

Animal experiment. The study involved 60 8-weeks old Syrian hamsters divided in 4 experimental groups of 15 individuals each (infected and mock females and males). Animals were acclimatized 7 days prior to infection in individual cages (BCU-2 Rat Sealed Negative Pressure IVC, Allentown Inc) within the biosafety level 3 (BSL3) facility, following national and international regulations on the welfare of laboratory animals.
Animals were inoculated intranasally under general anesthesia with Isoflurane using $8x10^4$ PFU/100µl of SARS-CoV-2, B.1.1.7 variant (Accession N: EPI_ISL_766579)[74]. Control animals were inoculated using 100µl of sterile PBS solution.
Animals were daily monitored for 14 days to record clinical signs. At 2, 4, 6, 9 and 14 dpi we registered weights and collected oropharyngeal swabs and blood samples from the gingival vein under general anesthesia[75]. At day 2, 6 and 14 we euthanized 5 individuals per group and performed an intra-cardiac terminal blood collection for PBMCs isolation with Ficoll-Paque Plus (GE healthcare) (Supplementary Fig. 3). We performed a complete necropsy of all animals and collected samples of the lungs, brains and intestines. Specimens were fixed in 10% neutral-buffered formalin and in RNA later (Thermo Fisher®) for histological examination and molecular analyses respectively. Further details can be found as supplementary materials.

Histology and immunofluorescence. Formalin fixed samples were paraffin-embedded, cut in 4µm-thick sections and stained with hematoxylin and eosin (H&E) to evaluate the presence and severity of lesions in different organs. Histological lesions were scored according to[38] (Supplementary Table 1). Slides were analyzed and images were taken using a Leica DM4 B light microscope with a DFC450 C Microscope Digital Camera at 20X and the software Leica Application Suite V4.13 (Leica Microsystems, Wetzlar, Germany).
We investigated the presence of the virus within tissues by immunofluorescence, using anti-SARS-CoV-2 spike glycoprotein and anti-dsRNA[46,76] as primary antibodies in order to discriminate the presence of the antigen by the active replication of the virus within tissues, based on the fact that dsRNA is widely known as replicative intermediate for coronaviruses[47]. Immunofluorescence was also applied to investigate the expression of the ACE-2 receptors within tissues. Further details can be found as supplementary materials and in Supplementary Table 6.

Molecular analyses for SARS-CoV-2 detection and quantification. The presence of viral RNA in oropharyngeal swabs was determined in all the control and infected individuals by qualitative rRT-PCR using the AgPath-ID™ One-Step RT-PCR Reagents (Life Technologies) on a CFX96 Touch Deep Well Real-time PCR Detection System (Biorad). To quantify SARS-CoV-2 in target organs, we developed a digital droplet RT-PCR (RT-ddPCR) employing the One-Step RT-ddPCR Advanced Kit for Probes (Bio-Rad) and the QX200 Droplet Digital PCR System (Biorad). This approach was implemented only for the three individuals per experimental group that were randomly selected for transcriptomic analyses. Quantitative data were expressed as Log2 genome copies (GC)/ml RNA. Both tests targeted SARS-CoV-2 envelope protein (E) gene[77]. The quality of the samples was verified by amplification of the β-actin mRNA[78]. Further details can be found as supplementary materials.

Gene expression analyses by RNA-Seq. We randomly selected three individuals among five of each experimental group to investigate virus-host response by performing the transcriptomic profile of the lungs, brains, intestines and PBMCs of infected *versus* mock

animals at three different time points along the infection, representing early infection, the infection apex and recovery.
Libraries were prepared with the Truseq Stranded mRNA library preparation kit (Illumina), following manufacturer's instructions and were run on an Agilent 2100 Bioanalyzer using an Agilent High Sensitivity DNA kit (Agilent Technologies) to ensure the proper range of cDNA length distribution. Sequencing was performed on Illumina NextSeq with NextSeq® 500/550 High Output Kit v2.5 (300 cycles; Illumina) in pair-end [PE] read mode producing about 33 million reads per sample. After filtering raw data, we aligned high-quality reads against the reference genome of *Mesocricetus auratus* (BCM Maur 2.0, NCBI)[79] using STAR v2.7.9a[80] and generated the gene count using htseq-count v0.11.0[81]. We then investigated the differential expression of genes between infected and mock males and females at each time point with Deseq2 package[82] and assigned Gene Ontology (GO) terms to each gene using Blast2GO v5.2.5[83]. Child-father relationships belonging to GO graph were reconstructed using the OBO file downloaded from http://geneontology.org/ (accessed on 19/10/2021). Orthologs with *Homo sapiens*, *Mus musculus* and *Rattus norvegicus* were computed using Orthofinder v2.5.4[84] and their proteome downloaded from Ensembl. Further details can be found as supplementary materials.

Serological analyses. In order to evaluate sero-conversion dynamics, we performed the focus reduction neutralization test (FRNT) as previously described, using for the detection of neutralizing antibodies the same viral strain used for the infection[85,86]. We defined as serum neutralization titer the reciprocal of the highest dilution resulting in a reduction of the control focus count higher than 90% (FRNT90). Sera of all animals were collected at 2, 4, 6, 9 and 14dpi; only 4 out of 5 sera were collected for both males and females at 9 dpi.
We further analyzed serum samples of all the controls and infected animals at 2, 4, 6, 9 and 14dpi for the presence of pro-inflammatory cytokines. Levels of IL-1β and IL-6 were assessed at the Istituto Zooprofilattico Sperimentale della Sardegna through singleplex ELISA using target-specific ELISA kits (MyBiosource), according to the manufacturers' instructions and using an Epoch microplate reader (BioTek) to read absorbance.

Statistical analyses. We adopted the minimum sample size that guaranteed effective comparison while minimizing the use of experimental animals. Infection of 13 out of 15 individuals per group indicated successful infection with a first type error $\alpha=0.01$ (one tail) and a power $1-\beta=0.85$.
To summarize viral shedding in males and females and to record changes in hamsters' weights during infection of males and females *versus* the corresponding group of mock animals, we performed descriptive statistical analysis using SAS 9.4 software[87–89]. We applied a spline mixed model by sex, taking into account the correlation among observation of the same hamster over time using a first-order autoregressive AR(1) structure for the covariance matrix (see supplemental materials for further details on the model). For all the remaining statistical analyses, we used a Mann-Whitney test for independent parameters implemented in GraphPad Prism 9. These included comparison between mean antibody titers and serum levels of IL-1β and IL-6 of females *versus* males at each time point and between histological scores of infected *versus* mock animals of each sex at 2, 6 and 14 dpi. For all statistics, we considered as significant P-values < 0.05.

Data availability

RNA-Seq raw data generated for the present study were deposited in SRA under accession number PRJNA839918. Source data for Figures 1a-b; 2d-f; 3a-c; 4a-c; 5a–b; 6ba, c are provided as supplementary tables.

Ethical statement

Animal studies were performed in compliance with directive 2010/63/EU of the European Parliament and of the Council of 22 September 2010 on the protection of animals used for scientific purposes. The experimental design was approved by IZSVe ethical board and by the Italian Ministry of Health, under permit n. 1167/2020-PR. In accordance with the 3Rs principle (Replacement, Reduction and Refinement), we used the minimum number of animals that secured statistically sound results and provided best housing and environmental enrichment. Briefly, individual housing exceeded the minimum surface required and agreed with the ecology, behavior and biology of the species. Temperature, humidity and light-dark cycles were fixed (21 ± 3 °C, 50 ± 10%, lights off: 07:00 AM–07:00 PM) and monitored throughout the study. All animals had *ad libitum* access to food and water throughout the entire study. Environmental enrichment consisted of gnawing blocks, nesting material and extra sunflower seeds three times a week. We guaranteed daily monitoring of animals' health and comfort and established a humanitarian threshold to avoid unnecessary suffering.
Animals were bred *in house* at the Istituto Zooprofilattico Sperimentale delle Venezie, under permission N n°2020/0095 granted by the municipality of Legnaro on August 2020.

Funding

The present work was supported by the Italian Ministry of Health through the grant IZSVE 01/20 RCS.

Acknowledgements

The authors would like to thank Francesco Bonfante to kindly provide the viral strain used in this study. We acknowledge Massimo Boldrin, Franco Mutinelli, Maria Augusta Bozza and the whole team of IZSVE's animal facilities for their support in the breeding and management of hamsters. We also thank Annalisa Salviato, Alessia Schivo, Miriam Abbadi, Lorena Biasini, Sara Petrin and Arianna Peruzzo for their training, support and precious suggestions on wet lab techniques for transcriptomic analyses. We also thank Giorgia Monetti for processing fixed organs and providing tissue slices for immunofluorescence and histological analyses. Finally, we are grateful to Francesca Ellero for her English edits on the manuscript.

Author Contributions

Funding acquisition and project administration: C.T., P.D.B and S.L.; supervision: S.C. and P.D.B.; resources: A.O., M.V., I.M., C.T. and P.D.B.; study design: M.C., G.Z., M.M., P.D.B., and S.L.; animal experiments: M.C., M.Z., P.D., P.D.B. and S.L.; histology: Gr.F. and M.V.; molecular analyses: M.C., P.D., I.B. and V.P.; immunofluorescence: M.C.; transcriptomic analyses: M.C. and G.Z.; serology: A.B. and M.P.; ELISA: Gi.F.; statistics: M.M.; data interpretation: M.C., G.Z., Gr. F., Gi.F., S.C., P.D.B. and S.L.; writing (first draft): M.C., G.Z., Gr.F, Gi.F., M.M., V.P. and S.L.; writing (revision): all authors; Figures: M.C., G.Z., Gr.F., Gi.F., M.M. and S.L.

Competing interests

The authors declare no competing interests.

Figures and figure legends

Figure 1. SARS-CoV-2 infection in oropharyngeal swabs, lungs and distal organs. a, Statistical model describing body weight changes in mock and infected male (Mock M, M) and female (Mock F, F) Syrian hamsters. **b**, Statistical model describing rRT-PCR results trend of RNA extracted from oropharyngeal swabs at 2, 4, 6, 9 and 14 dpi. **a-b**, Fig. 1 a-b: infected and control females 2 dpi n = 30; 4 dpi n = 20; 6 dpi n = 20; 9 dpi n = 10; 14 dpi n = 10 infected and control males 2 dpi n = 30; 4 dpi n = 20; 6 dpi n = 20; 9 dpi n = 10; 14 dpi n = 10. See Supplementary Table 1 for further details. **c**, Focus reduction neutralization test (FRNT), expressed as the reciprocal of the highest dilution resulting in a reduction of the control focus count > 90% (FRNT90). Geometric means (GMT) with 95% confidence intervals (CI) are represented. Dotted line indicate the limit of detection (LOD). Mann-Whitney test male vs females; 2dpi $P > 0.99$, 4dpi $P > 0.99$, 6dpi $P = 0.16$, 9dpi $P = 0.63$, 14dpi $P = 0.59$. Infected females 2 dpi n = 5; 4 dpi n = 5; 6 dpi n = 5; 9 dpi n = 4; 14 dpi n = 5 infected males 2 dpi n = 5; 4 dpi n = 5; 6 dpi n = 5; 9 dpi n = 4; 14 dpi n = 5. **d**, SARS-CoV-2 viral load as determined by RT-ddPCR in the lungs, intestines and brains at 2, 6 and 14 dpi; results are expressed as Log2 of Genomic Copies (GC)/ml for graphical comparison between organs. Infected female and male lungs and intestines: 2, 6 and 14 dpi n = 3 each infected female and male brains: 2 dpi n = 3; 6 dpi n = 2; 14 dpi n = 3 each. **e**, Representative immunofluorescence staining for SARS-CoV-2 Spike glycoprotein (green) and dsRNA (red) in infected male and female lungs. Scale bar = 25μm. All animals were analyzed, representative images are shown.

Figure 2. SARS-CoV-2 infection results in severe but rapidly resolving pulmonary lesions in male and female Syrian hamsters. a, **b**, and **c**, Representative images of Syrian hamster lungs collected at 2, 6 and 14 dpi and mock animals. H&E stained sections. Scale bar = 200 μm. All animals were analyzed, representative images are shown. **d**, Cumulative score of lung pathology for nine histopathological assessments in male and female hamsters (Supplementary Table 2); mean values ± SD are represented. Mann-Whitney test males vs females; 2dpi $P = 0.86$, 6dpi $P = 0.31$, 14dpi $P = 0.72$. **e** and **f**, Histopathological scores of intra-alveolar inflammatory cell infiltration and perivascular/alveolar edema in males and female hamsters (Supplementary Table 2; all animals were analyzed). Mean values ± SD are represented. Mann-Whitney test mock animals vs females of total histopathological score (2dpi $P = 0.0007$, 6dpi $P = 0.0003$, 14dpi $P = 0.0003$), intra-alveolar inflammatory cell infiltration (2dpi $P = 0.0003$, 6dpi $P = 0.0003$, 14dpi $P = 0.0003$) and perivascular/alveolar edema (2dpi $P > 0.99$, 6dpi $P = 0.0003$, 14dpi = 0.52). Mann-Whitney test mock animals vs males of total histopathological score (2dpi $P = 0.0007$, 6dpi $P = 0.0003$, 14dpi $P = 0.0003$), intra-alveolar inflammatory cell infiltration (2dpi $P = 0.0003$, 6dpi $P = 0.0003$, 14dpi $P = 0.0003$) and perivascular/alveolar edema (2dpi $P = 0.19$, 6dpi $P = 0.0003$, 14dpi > 0.99). Mann-Whitney test male vs females of total histological score (2dpi $P = 0.86$, 6dpi $P = 0.31$, 14dpi $P > 0.72$), intra-alveolar inflammatory cell infiltration (2dpi $P > 0.99$, 6dpi $P = 0.21$, 14dpi $P > 0.99$) and perivascular/alveolar edema (2dpi $P = 0.40$, 6dpi $P = 0.12$, 14dpi > 0.99). * indicates a statistically significant comparison. **g**, **1**, Severe bronchiolar epithelium and pneumocyte II hyperplasia at 6 dpi; nuclei of proliferating cells were frequently megalic with prominent nucleoli and numerous mitotic figures. **2**, A syncytial epithelial cell containing multiple 2-4 μm amphophilic round cytoplasmic viral-like inclusions, in a male hamster at 6 dpi. **3**, Lymphomonocytic endothelialitis and perivascular cuffing in a pulmonary venule at 6 dpi. **4**, Alveolar bronchiolization with acinar formations and few interstitial lymphoplasmacytic infiltration at 14 dpi. H&E stained sections. Images were acquired with a Leica DM4 B light microscope with a DFC450 C Microscope Digital Camera and the software Leica Application Suite V4.13 (Leica Microsystems). Scale bar = 50μm.

Figure 3. RNA-Seq global expression profiles. a, Volcano and MA plot showing differential expression analysis results for lungs/intestine/brains and PBMCs, respectively (blue, up-regulated; red, down-regulated; gray, not significant). A DEG is significant in a comparison when Log2FC≤-1 or Log2FC≥1and FDR<0.05. For lungs, intestines and brains: x axis = Log2FC; y axis = -LogFDR. For PBMCs: x axis = Log mean expression; y axis = Log2FC. **b**, Number of DEGs for every comparison infected vs mock, done in differential expression analysis; up- and down-regulated genes are shown. See also Supplementary Table 4 for DEGs numbers. **c**, Number of enriched GO terms for every comparison infected vs mock done in Gene Ontology enrichment analysis. See also Supplementary Table 5 for GO terms numbers. Infected female and male lungs and intestines: 2, 6 and 14 dpi n = 3 each; infected female and male brains: 2 dpi n = 3; 6 dpi n = 2; 14 dpi n = 3 each; infected female and male PBMCs: a pool of 5 animals' blood was analyzed at each time point.

Figure 4. Transcriptomic profile of SARS-CoV-2 infected male and female Syrian hamsters. a, Dotplot representing the most specific enriched Gene Ontology (GO) terms related to immunity in lungs. **b**, Dotplot representing the most specific enriched GO terms related to immunity in intestine. **c**, Dotplot representing the most specific enriched GO terms related to immunity in brain. Statistically significant enrichments (FDR<0.05) are presented and -LogFDR is shown.

598 **Figure 5. Transcriptomic profile of SARS-CoV-2 infected male and female PBMCs. a**,
599 Dotplot representing the most specific enriched GO terms related to immunity in PBMCs.
600 Statistically significant enrichments (FDR<0.05) are presented and –LogFDR is shown. **b**,
601 Scatterplot representing the Log2FC of males and females DEGs in PBMCs at 14 dpi. DE =
602 Differentially expressed. A DEG is significant in a comparison when Log2FC≤-1 or
603 Log2FC≥1and FDR<0.05.
604

Figure 6. Transcriptomic analysis highlights differences in males and females systemic response to SARS-CoV-2 infection. a, Heatmap (Log2FC values of the performed comparisons) of selected genes related to the immune system in the lungs. A DEG is significant in a comparison when Log2FC≤-1 or Log2FC≥1and FDR<0.05. **b**, Immunofluorescence staining for SARS-CoV-2 receptor ACE2 in infected and control males and females lungs at 6 dpi; all animals were analyzed, representative images are shown. Scale bar = 25µm. **c**, Heatmap (Log2FC values of the performed comparisons) of selected genes related to the immune system in the PBMCs transcriptome. *indicates the gene name for hamsters in case it differs from the human ortholog. **d**, Singleplex ELISA levels (pg/mL) for mock and infected male and female hamsters IL-1β. Mann-Whitney tests of mock or SARS-CoV-2 M vs F; mean ± SEM is represented (* indicates a statistically significant comparison).

References

1. Zhu, N. *et al.* A Novel Coronavirus from Patients with Pneumonia in China, 2019. *N. Engl. J. Med.* **382**, 727–733 (2020).

2. Berlin, D. A., Gulick, R. M. & Martinez, F. J. Severe Covid-19. *N. Engl. J. Med.* **383**, 2451–2460 (2020).

3. Gandhi, R. T., Lynch, J. B. & del Rio, C. Mild or Moderate Covid-19. *N. Engl. J. Med.* **383**, 1757–1766 (2020).

4. Zhang, T., Wu, Q. & Zhang, Z. Probable Pangolin Origin of SARS-CoV-2 Associated with the COVID-19 Outbreak. *Curr. Biol.* **30**, 1346-1351.e2 (2020).

5. Holmes, E. C. *et al.* The origins of SARS-CoV-2: A critical review. *Cell* **184**, 4848–4856 (2021).

6. Fullard, J. F. *et al.* Single-nucleus transcriptome analysis of human brain immune response in patients with severe COVID-19. *Genome Med.* **13**, 1–13 (2021).

7. Spudich, S. & Nath, A. Nervous system consequences of COVID-19. **375**, 267–270 (2022).

8. Chen, Z. R. *et al.* COVID-19 and gastroenteric manifestations. *World J. Clin. Cases* **9**, 4990–4997 (2021).

9. Gagliardi, S. *et al.* Detection of SARS-CoV-2 genome and whole transcriptome sequencing in frontal cortex of COVID-19 patients. *Brain. Behav. Immun.* **97**, 13–21 (2021).

10. Soltani Zangbar, H., Gorji, A. & Ghadiri, T. A Review on the Neurological Manifestations of COVID-19 Infection: a Mechanistic View. *Mol. Neurobiol.* **58**, 536–549 (2021).

11. Arunachalam, P. S. *et al.* Systems biological assessment of immunity to mild versus severe COVID-19 infection in humans. *Science (80-.).* **6261**, eabc6261 (2020).

12. Tay, M. Z., Poh, C. M., Rénia, L., MacAry, P. A. & Ng, L. F. P. The trinity of COVID-19: immunity, inflammation and intervention. *Nat. Rev. Immunol.* **20**, 363–374 (2020).

13. Lamers, M. M. & Haagmans, B. L. SARS-CoV-2 pathogenesis. *Nat. Rev. Microbiol.* **20**, (2022).

14. Beltrame, A. *et al.* Association Between Sex Hormone Levels and Clinical Outcomes in Patients With COVID-19 Admitted to Hospital: An Observational, Retrospective, Cohort Study. *Front. Immunol.* **13**, 1–10 (2022).

15. Stanelle-Bertram, S. *et al.* SARS-CoV-2 induced CYP19A1 expression in the lung correlates with increased aromatization of testosterone-to-estradiol in male golden hamsters. (2020).

16. Takahashi, T. *et al.* Sex differences in immune responses that underlie COVID-19 disease outcomes. *Nature* (2020) doi:10.1038/s41586-020-2700-3.

17. Zhang, B. *et al.* Clinical characteristics of 82 cases of death from COVID-19. *PLoS One* **15**, (2020).

18. Mohamed, L., Rokni, M., Mokhtari, T. & Noorbakhsh, F. Immunology, immunopathogenesis and immunotherapeutics of COVID-19; an overview. *Int. Immunopharmacol.* **93**, (2021).

19. Yang, Y. *et al.* Plasma IP-10 and MCP-3 levels are highly associated with disease severity and predict the progression of COVID-19. *J. Allergy Clin. Immunol.* **146**, 119-127.e4 (2020).

20. Russell, C. D. Exploiting an early immunological window of opportunity in COVID-19. *Lancet Respir. Med.* **9**, 811–812 (2021).

21. Harvey, W. T. *et al.* SARS-CoV-2 variants, spike mutations and immune escape. *Nat. Rev. Microbiol.* **19**, 409–424 (2021).

22. Graham, M. S. *et al.* Changes in symptomatology, reinfection, and transmissibility associated with the SARS-CoV-2 variant B.1.1.7: an ecological study. *Lancet Public Heal.* **6**, e335–e345 (2021).

23. Curran, J. *et al.* Transmission characteristics of SARS-CoV-2 variants of concern. *Rev. medRxiv* **2021**, 2021.04.23.21255515 (2021).

24. Vellas, C. *et al.* Influence of treatment with neutralizing monoclonal antibodies on the SARS-CoV-2 nasopharyngeal load and quasispecies. *Clin. Microbiol. Infect.* **28**, 139.e5-139.e8 (2022).

25. Hwang, Y. C. *et al.* Monoclonal antibodies for COVID-19 therapy and SARS-CoV-2 detection. *J. Biomed. Sci.* **29**, 1–50 (2022).

26. VanBlargan, L. A. *et al.* An infectious SARS-CoV-2 B.1.1.529 Omicron virus escapes neutralization by therapeutic monoclonal antibodies. *Nat. Med.* **28**, 490–495 (2022).

27. Thakur, S. *et al.* SARS-CoV-2 Mutations and Their Impact on Diagnostics, Therapeutics and Vaccines. *Front. Med.* **9**, (2022).

28. Yin, J. *et al.* Advances in the development of therapeutic strategies against COVID-19 and perspectives in the drug design for emerging SARS-CoV-2 variants. *Comput. Struct. Biotechnol. J.* **20**, 824–837 (2022).

29. Chakraborty, C., Bhattacharya, M. & Sharma, A. R. Emerging mutations in the SARS-CoV-2 variants and their role in antibody escape to small molecule-based therapeutic resistance. *Curr. Opin. Pharmacol.* (2020).

30. Shi, J. *et al.* Susceptibility of ferrets, cats, dogs, and different domestic animals to SARS-coronavirus-2. 1–23 (2020).

31. Rockx, B. *et al.* Comparative Pathogenesis Of COVID-19, MERS And SARS In A

Non-Human Primate Model. *Science (80-.).* **7314**, (2020).

32. Sia, S. F. *et al.* Pathogenesis and transmission of SARS-CoV-2 in golden hamsters. *Nature* **583**, 834–838 (2020).

33. Chan, A. J. F., Zhang, A. J., Yuan, S. & Kwok-, V. Simulation of the clinical and pathological manifestations of Coronavirus Disease 2019 (COVID-19) in golden Syrian hamster model: implications for disease pathogenesis and transmissibility. **2019**, 1–50 (2019).

34. Shou, S. *et al.* Animal Models for COVID-19: Hamsters, Mouse, Ferret, Mink, Tree Shrew, and Non-human Primates. *Front. Microbiol.* **12**, (2021).

35. Imai, M. *et al.* Syrian hamsters as a small animal model for SARS-CoV-2 infection and countermeasure development. *Proc. Natl. Acad. Sci. U. S. A.* **117**, 16587–16595 (2020).

36. Muñoz-Fontela, C. *et al.* Animal models for COVID-19. *Nature* (2020) doi:10.1038/s41586-020-2787-6.

37. Armando, F. *et al.* SARS-CoV-2 Omicron variant causes mild pathology in the upper and lower respiratory tract of hamsters. *Nat. Commun.* **13**, (2022).

38. Hoagland, D. A. *et al.* Leveraging the antiviral type I interferon system as a first line of defense against SARS-CoV-2 pathogenicity. *Immunity* **54**, 557-570.e5 (2021).

39. Osterrieder, N. *et al.* Age-dependent progression of SARS-CoV-2 infection in syrian hamsters. *Viruses* **12**, 1–5 (2020).

40. O'Donnell, K. L. *et al.* Pathogenic and transcriptomic differences of emerging SARS-CoV-2 variants in the Syrian golden hamster model. *EBioMedicine* **73**, 1–32 (2021).

41. Hansen, F. *et al.* SARS-CoV-2 reinfection prevents acute respiratory disease in Syrian hamsters but not replication in the upper respiratory tract. *Cell Rep.* **38**, 110515 (2022).

42. Warner, B. M., Safronetz, D. & Kobinger, G. P. Syrian Hamsters as a Small Animal Model for Emerging Infectious Diseases: Advances in Immunologic Methods. *Advs Exp. Med. Biol. Microbiol. Infect. Dis. Public Heal.* (2016) doi:10.1007/5584.

43. Lai, A. *et al.* Circulating SARS-CoV-2 variants in Italy, October 2020–March 2021. *Virol. J.* **18**, 1–5 (2021).

44. Stefanelli, P. *et al.* Co-circulation of SARS-CoV-2 Alpha and Gamma variants in Italy, February and March 2021. *Eurosurveillance* **27**, (2022).

45. Chan, J. F. W. *et al.* Simulation of the Clinical and Pathological Manifestations of Coronavirus Disease 2019 (COVID-19) in a Golden Syrian Hamster Model: Implications for Disease Pathogenesis and Transmissibility. *Clin. Infect. Dis.* **71**, 2428–2446 (2020).

46. Cao, H. *et al.* RNA binding protein 24 regulates the translation and replication of hepatitis C virus. *Protein Cell* **9**, 930–944 (2018).

47. Perlman, S. & Netland, J. Coronaviruses post-SARS: Update on replication and pathogenesis. *Nat. Rev. Microbiol.* **7**, 439–450 (2009).

48. Tostanoski, L. H. *et al.* Ad26 vaccine protects against SARS-CoV-2 severe clinical disease in hamsters. *Nat. Med.* **26**, 1694–1700 (2020).

49. Konopka, K. E. *et al.* Diffuse alveolar damage (DAD) resulting from coronavirus disease 2019 Infection is Morphologically Indistinguishable from Other Causes of DAD. *Histopathology* **77**, 570–578 (2020).

50. Veenhuis, R. T. & Zeiss, C. J. Animal Models of COVID-19 II. Comparative Immunology. *ILAR J.* **62**, 17–34 (2021).

51. Gruber, A. D., Firsching, T. C., Trimpert, J. & Dietert, K. Hamster models of COVID-19 pneumonia reviewed: How human can they be? *Vet. Pathol.* **59**, 528–545 (2022).

52. Yen, H.-L. *et al.* Transmission of SARS-CoV-2 (variant Delta) from pet hamsters to humans and onward human propagation of the adapted strain: a case study.

53. Dhakal, S. *et al.* Sex Differences in Lung Imaging and SARS-CoV-2 Antibody Responses in a COVID-19 Golden Syrian Hamster Model. *MBio* **12**, e0097421 (2021).

54. Tizard, I. Sickness behavior, its mechanisms and significance. *Anim. Health Res. Rev.* **9**, 87–99 (2008).

55. Del Valle, D. M. *et al.* An inflammatory cytokine signature predicts COVID-19 severity and survival. *Nat. Med.* **26**, 1636–1643 (2020).

56. Daamen, A. R. *et al.* Comprehensive transcriptomic analysis of COVID-19 blood, lung, and airway. *Sci. Rep.* **11**, 1–19 (2021).

57. Liu, J. *et al.* SARS-CoV-2 cell tropism and multiorgan infection. *Cell Discov.* **7**, 2–5 (2021).

58. Deshmukh, V., Motwani, R., Kumar, A., Kumari, C. & Raza, K. Histopathological observations in COVID-19: A systematic review. *J. Clin. Pathol.* **74**, 76–83 (2021).

59. Murira, A. & Lamarre, A. Type-I interferon responses: From friend to foe in the battle against chronic viral infection. *Front. Immunol.* **7**, 1–8 (2016).

60. García-Sastre, A. Ten Strategies of Interferon Evasion by Viruses. *Cell Host Microbe* **22**, 176–184 (2017).

61. Blanco-Melo, D. *et al.* Imbalanced host response to SARS-CoV-2 drives development of COVID-19. *Cell* 1–10 (2020) doi:10.1016/j.cell.2020.04.026.

62. Kinoshita, T. *et al.* Co-infection of SARS-CoV-2 and influenza virus causes more severe and prolonged pneumonia in hamsters. *Sci. Rep.* **11**, 1–11 (2021).

63. Yang, S. J. *et al.* Characterization of virus replication, pathogenesis, and cytokine responses in syrian hamsters inoculated with sars-cov-2. *J. Inflamm. Res.* **14**, 3781–3795 (2021).

64. Coomes, E. A. & Haghbayan, H. Interleukin-6 in Covid-19: A systematic review and meta-analysis. *Rev. Med. Virol.* **30**, 1–9 (2020).

65. Lamers, M. M. *et al.* SARS-CoV-2 productively infects human gut enterocytes. *Science (80-.).* **369**, 50–54 (2020).

66. Qi, S. *et al.* Sex differences in the immune response to acute COVID-19 respiratory tract infection. *Biol. Sex Differ.* **12**, 1–10 (2021).

67. Jin, J. M. *et al.* Gender Differences in Patients With COVID-19: Focus on Severity and Mortality. *Front. Public Heal.* **8**, 1–6 (2020).

68. Peckham, H. *et al.* Male sex identified by global COVID-19 meta-analysis as a risk factor for death and ITU admission. *Nat. Commun.* **11**, 1–10 (2020).

69. Su, Y. J., Kuo, K. C., Wang, T. W. & Chang, C. W. Gender-based differences in COVID-19. *New Microbes New Infect.* **42**, 1–6 (2021).

70. Griffin, B. D. *et al.* Host parameters and mode of infection influence outcome in SARS-CoV-2-infected hamsters. *iScience* **24**, 103530 (2021).

71. Yuan, L. *et al.* Gender associates with both susceptibility to infection and pathogenesis of SARS-CoV-2 in Syrian hamster. *Signal Transduct. Target. Ther.* **6**, (2021).

72. Yang, L. *et al.* The signal pathways and treatment of cytokine storm in COVID-19. *Signal Transduct. Target. Ther.* **6**, 1–20 (2021).

73. Lee, S. K. Sex as an important biological variable in biomedical research. *BMB Rep.* **51**, 167–173 (2018).

74. Giobbe, G. G. *et al.* SARS-CoV-2 infection and replication in human gastric organoids. *Nat. Commun.* **12**, 1–14 (2021).

75. Rodrigues, M. V., De Castro, S. O., De Albuquerque, C. Z., De Moura Mattaraia, V. G. & Santoro, M. L. The gingival vein as a minimally traumatic site for multiple blood sampling in Guinea pigs & hamsters. *PLoS One* **12**, 1–16 (2017).

76. Leonova, K. *et al.* TRAIN (Transcription of repeats activates interferon) in response to chromatin destabilization induced by small molecules in mammalian cells. *Elife* **7**, 1–26 (2018).

77. Corman, V. *et al.* Detection of 2019 -nCoV by RT-PCR. *Euro Surveill* **25**, 1–8 (2020).

78. Gigante, C. M. *et al.* Multi-site evaluation of the LN34 pan-lyssavirus real-time RT-PCR assay for postmortem rabies diagnostics. *PLoS One* **13**, 1–25 (2018).

79. Harris, R. A. *et al.* Construction of a new chromosome-scale, long-read reference genome assembly of the Syrian hamster, Mesocricetus auratus. *bioRxiv* (2021).

80. Dobin, A. *et al.* STAR: Ultrafast universal RNA-seq aligner. *Bioinformatics* **29**, 15–21 (2013).

81. Anders, S., Pyl, P. T. & Huber, W. HTSeq-A Python framework to work with high-throughput sequencing data. *Bioinformatics* **31**, 166–169 (2015).

82. Love, M. I., Huber, W. & Anders, S. Moderated estimation of fold change and dispersion for RNA-seq data with DESeq2. *Genome Biol.* **15**, 1–21 (2014).

83. Conesa, A. & Götz, S. Blast2GO: A comprehensive suite for functional analysis in plant genomics. *Int. J. Plant Genomics* **2008**, (2008).

84. Emms, D. M. & Kelly, S. OrthoFinder: Phylogenetic orthology inference for comparative genomics. *Genome Biol.* **20**, 1–14 (2019).

85. Pagliari, M., Bonfante, F. & Padoan, A. Omicron neutralization and the inference of correlates of protection based on anti-SARS-CoV-2 S-RBD IgG levels in boosted individuals. (2022).

86. Padoan, A. *et al.* Analytical and clinical performances of a SARS-CoV-2 S-RBD IgG assay: Comparison with neutralization titers. *Clin. Chem. Lab. Med.* **59**, 1444–1452 (2021).

87. Cibin, V. *et al.* Usefulness of Escherichia coli and Enterobacteriaceae as Process Hygiene Criteria in poultry: experimental study. *EFSA Support. Publ.* **11**, (2017).

88. Roccato, A. *et al.* Usefulness of indicator bacteria as potential marker of Campylobacter contamination in broiler carcasses. *Int. J. Food Microbiol.* **276**, 63–70 (2018).

89. Petrin, S. *et al.* Effect of pH and Salinity on the Ability of Salmonella Serotypes to Form Biofilm. *Front. Microbiol.* **13**, (2022).

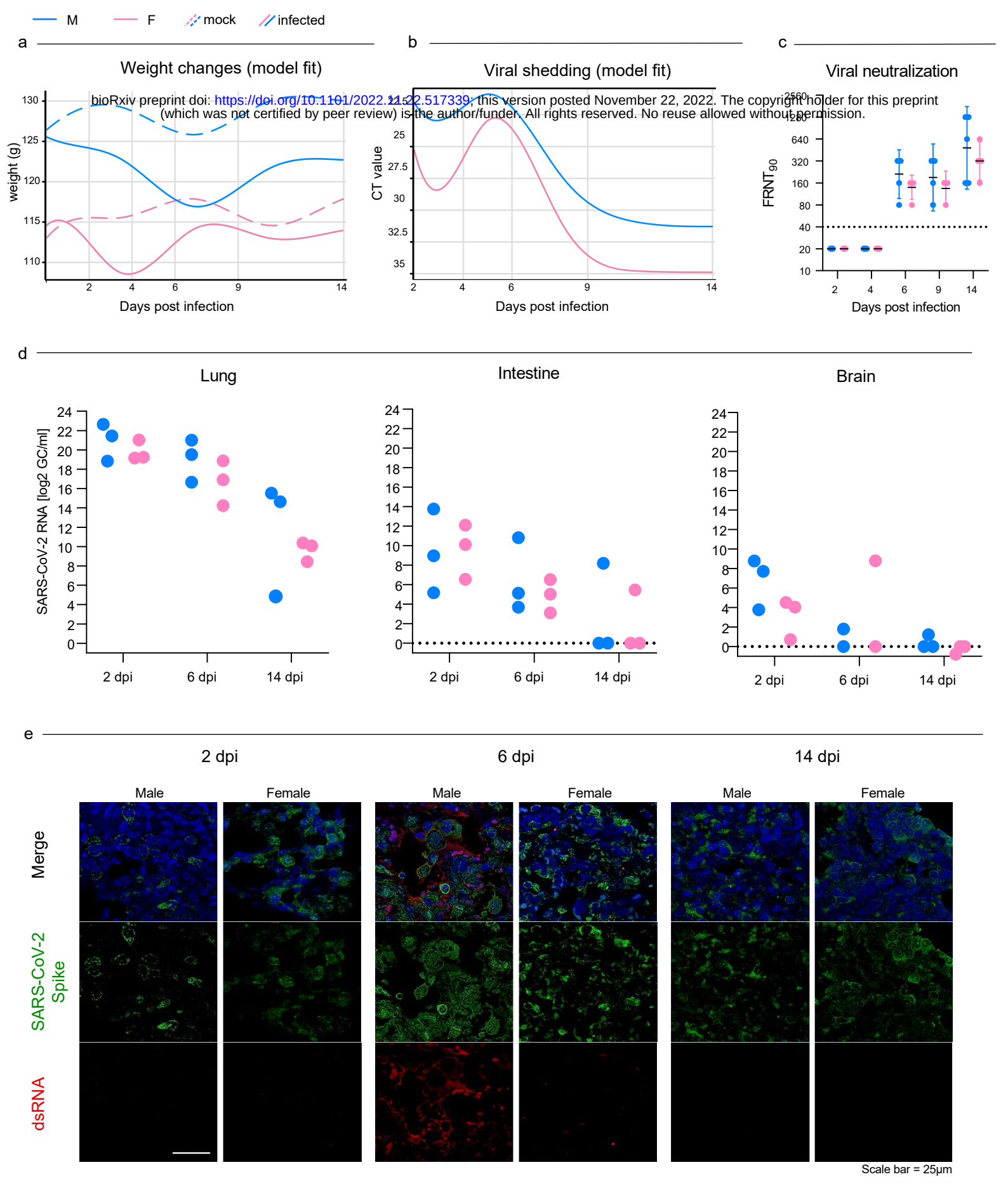

Figure 1

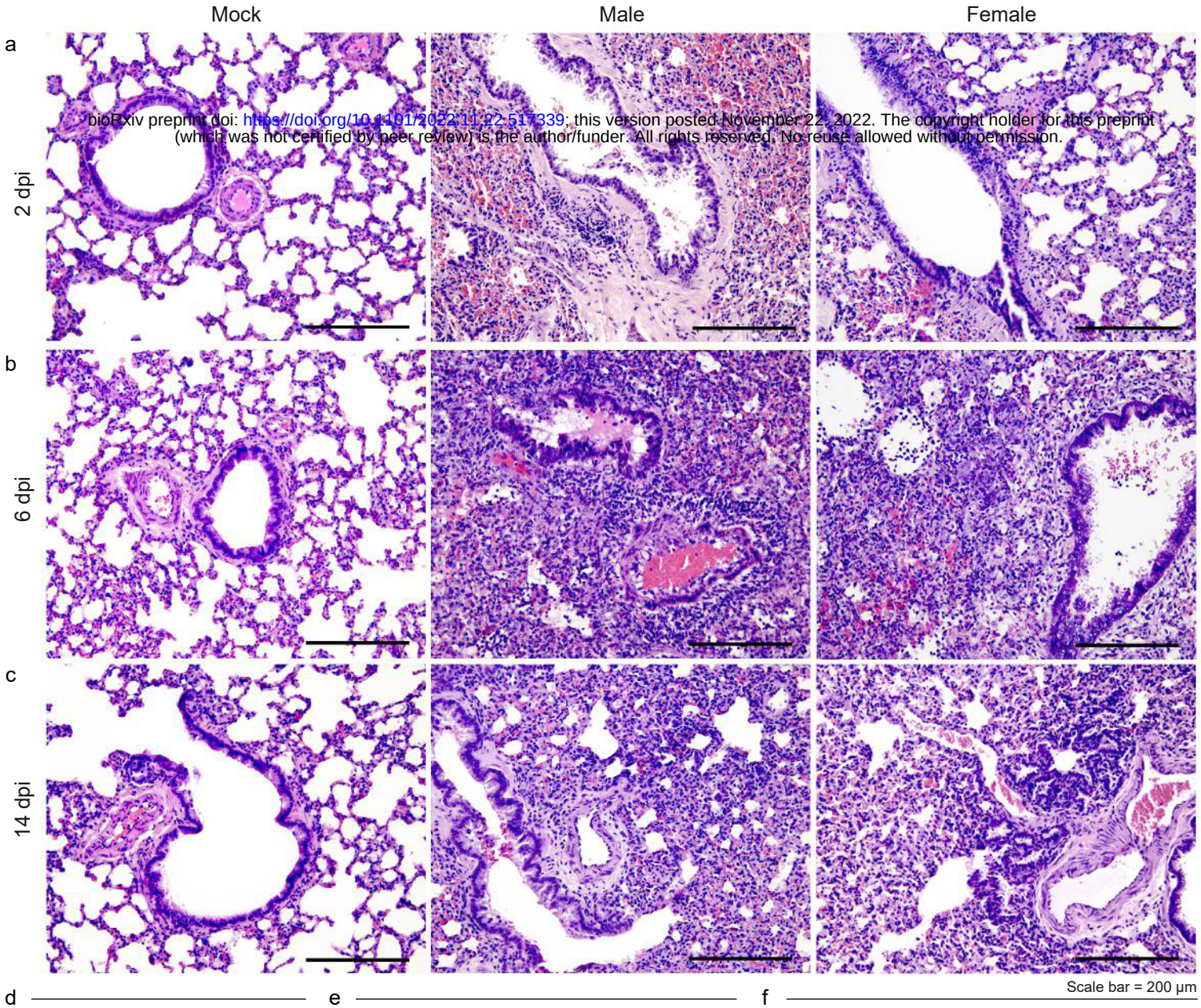

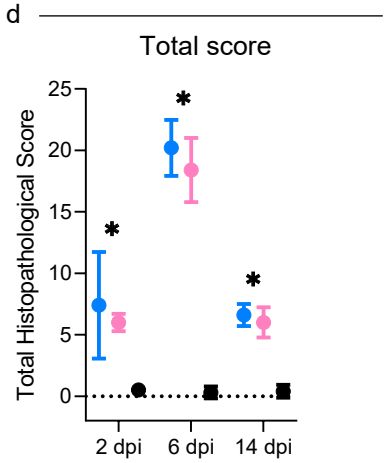

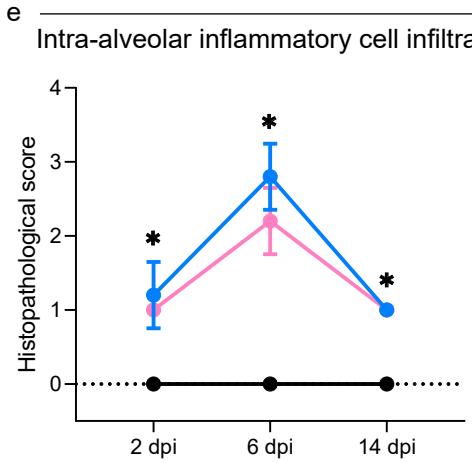

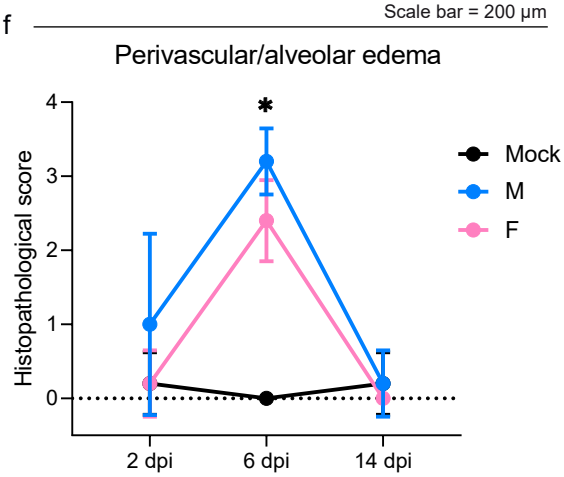

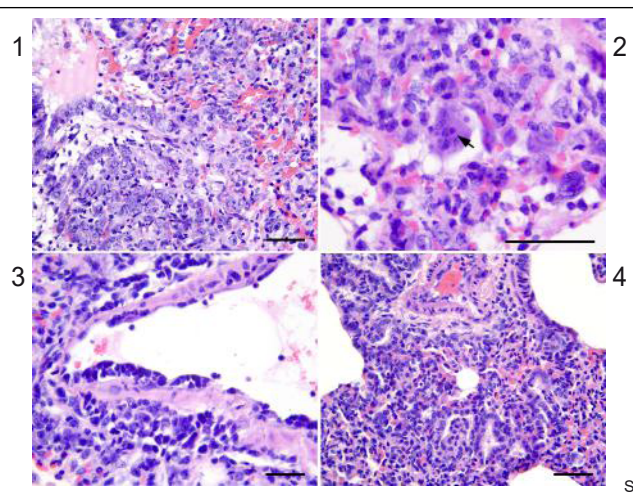

Figure 2

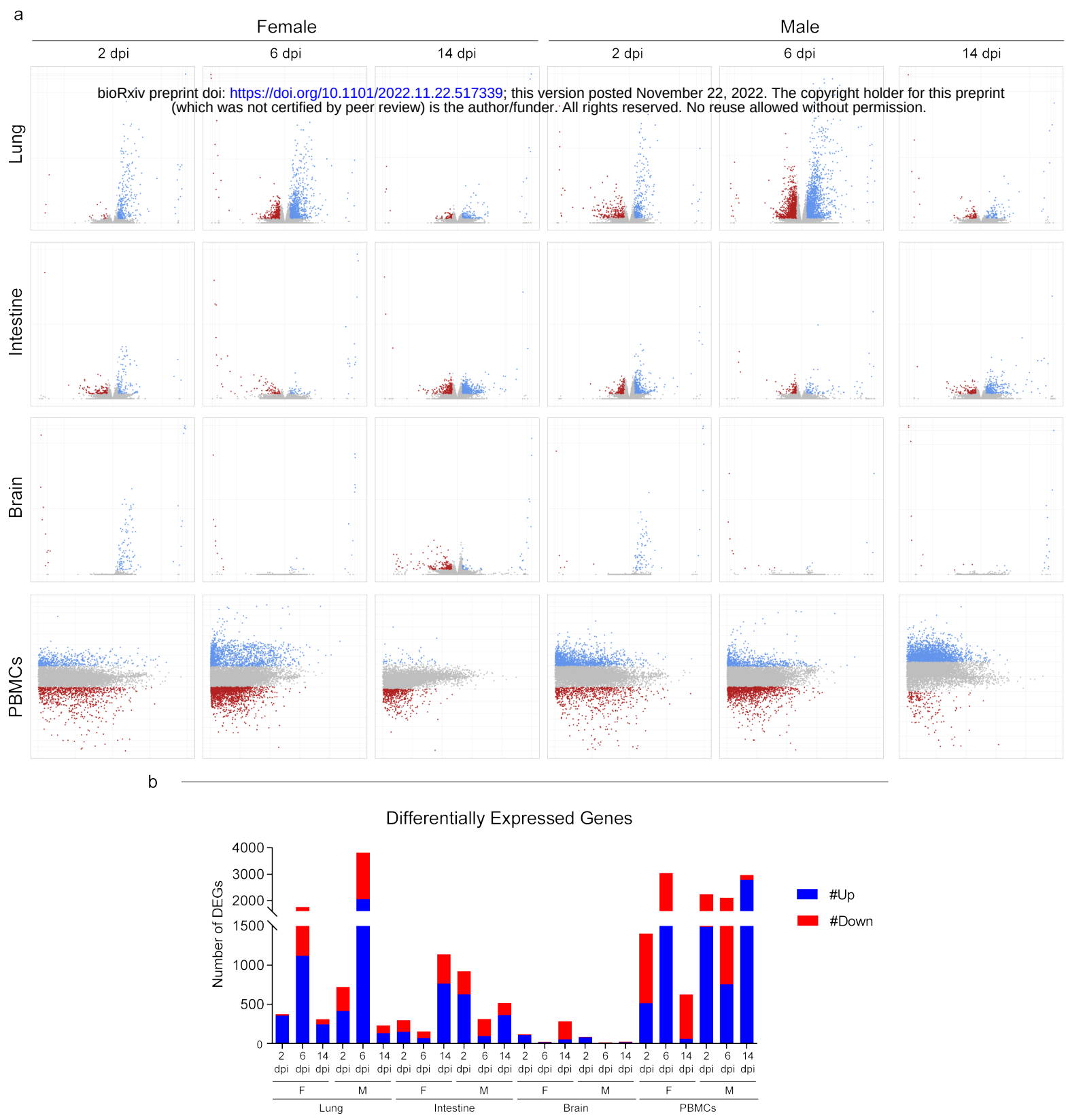

Figure 3


a
Lung
sex
timepoint
cellular response to type I IFN
inflammatory response
cellular response to IFN β
defense response to virus
activation of immune response
regulation of cytokine−mediated signaling pathway
cytokine−mediated signaling pathway
programmed cell death
wound healing
tissue regeneration
positive regulation of NK cell mediated immunity
T cell receptor signaling pathway
antigen receptor−mediated signaling pathway
mitotic cell cycle checkpoint signaling
response to INF γ
regulation of lymphocyte activation
leukocyte chemotaxis
cellular response to IFN α
antigen processing and presentation of peptide antigen via MHC class I
toll−like receptor signaling pathway
pattern recognition receptor signaling pathway
complement activation, classical pathway
humoral immune response mediated by circulating immunoglobulin
regulation of B cell differentiation
regulation of cytokine production
fatty acid metabolic process
actin nucleation
positive regulation of actin filament polymerization
angiogenesis
cytoplasmic translation
response to TNF
negative regulation of immune system process
microtubule−based movement
-Log (FDR)
>10
5
0
Fold enrichment
10
20
30
40
>50
sex
F
M
timepoint
2dpi
6dpi
14dpi
b
Intestine
sex
timepoint
positive regulation of innate immune response
cellular response to IFN α
wound healing
tissue regeneration
defense response to virus
inflammatory response
cytoskeleton organization
programmed cell death
antigen receptor−mediated signaling pathway
immune response−activating cell surface receptor signaling pathway
chemokine−mediated signaling pathway
cytokine−mediated signaling pathway
cellular response to IFN β
toll−like receptor signaling pathway
pattern recognition receptor signaling pathway
positive regulation of T cell differentiation
positive regulation of lymphocyte differentiation
B cell activation
c
Brain
sex
timepoint
activation of innate immune response
complement activation
defense response to virus
cellular response to IFN α
cellular response to IFN β
inflammatory response

Figure 4

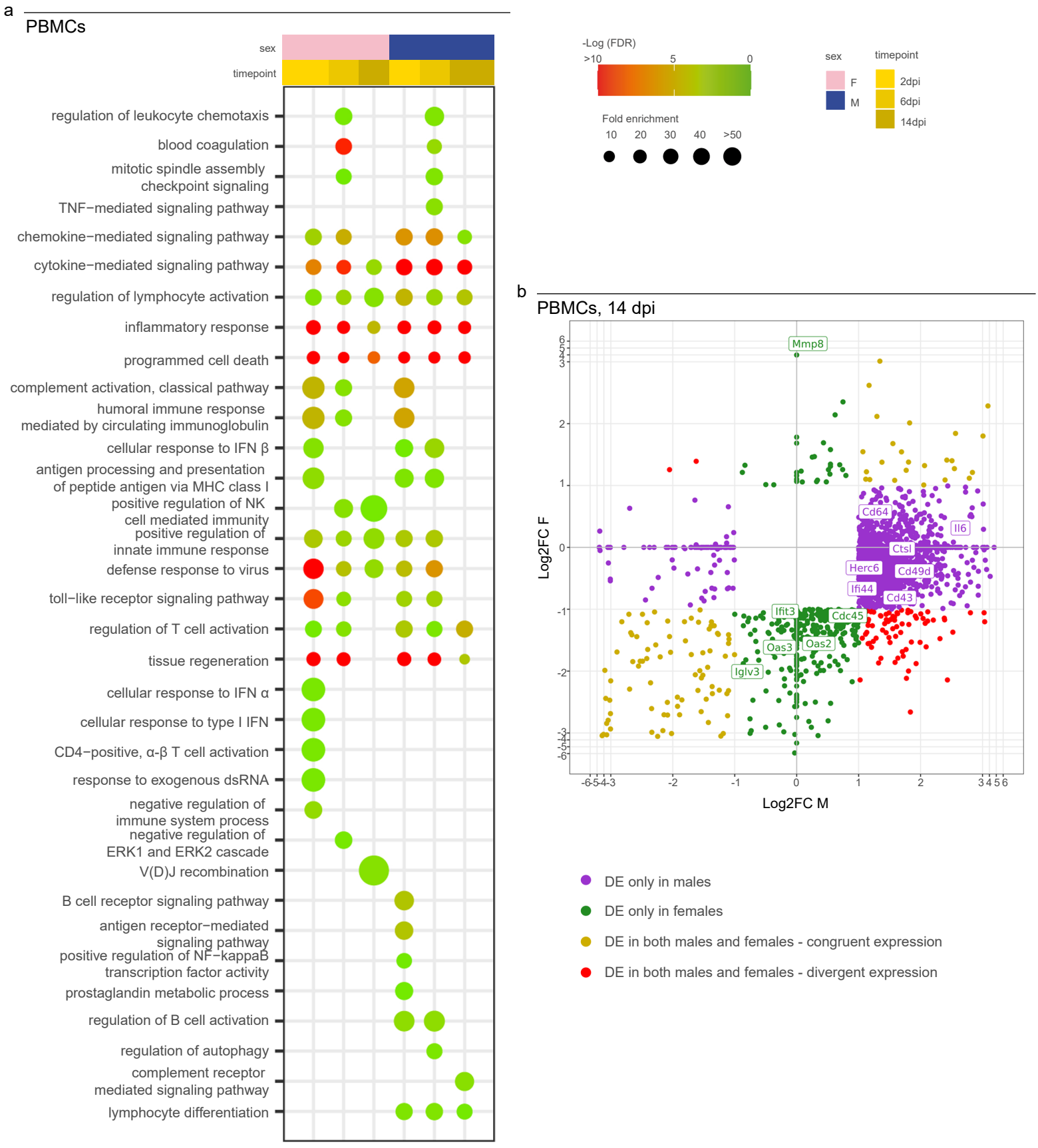
a
PBMCs
sex
timepoint
regulation of leukocyte chemotaxis
blood coagulation
mitotic spindle assembly checkpoint signaling
TNF−mediated signaling pathway
chemokine−mediated signaling pathway
cytokine−mediated signaling pathway
regulation of lymphocyte activation
inflammatory response
programmed cell death
complement activation, classical pathway
humoral immune response mediated by circulating immunoglobulin
cellular response to IFN β
antigen processing and presentation of peptide antigen via MHC class I
positive regulation of NK cell mediated immunity
positive regulation of innate immune response
defense response to virus
toll−like receptor signaling pathway
regulation of T cell activation
tissue regeneration
cellular response to IFN α
cellular response to type I IFN
CD4−positive, α-β T cell activation
response to exogenous dsRNA
negative regulation of immune system process
negative regulation of ERK1 and ERK2 cascade
V(D)J recombination
B cell receptor signaling pathway
antigen receptor−mediated signaling pathway
positive regulation of NF−kappaB transcription factor activity
prostaglandin metabolic process
regulation of B cell activation
regulation of autophagy
complement receptor mediated signaling pathway
lymphocyte differentiation
-Log (FDR)
>10
5
0
Fold enrichment
10
20
30
40
>50
sex
F
M
timepoint
2dpi
6dpi
14dpi
b
PBMCs, 14 dpi
Log2FC F
Log2FC M
Mmp8
Cd64
Il6
Ctsl
Herc6
Cd49d
Ifi44
Cd43
Ifit3
Cdc45
Oas3
Oas2
Iglv3
DE only in males
DE only in females
DE in both males and females - congruent expression
DE in both males and females - divergent expression

Figure 5

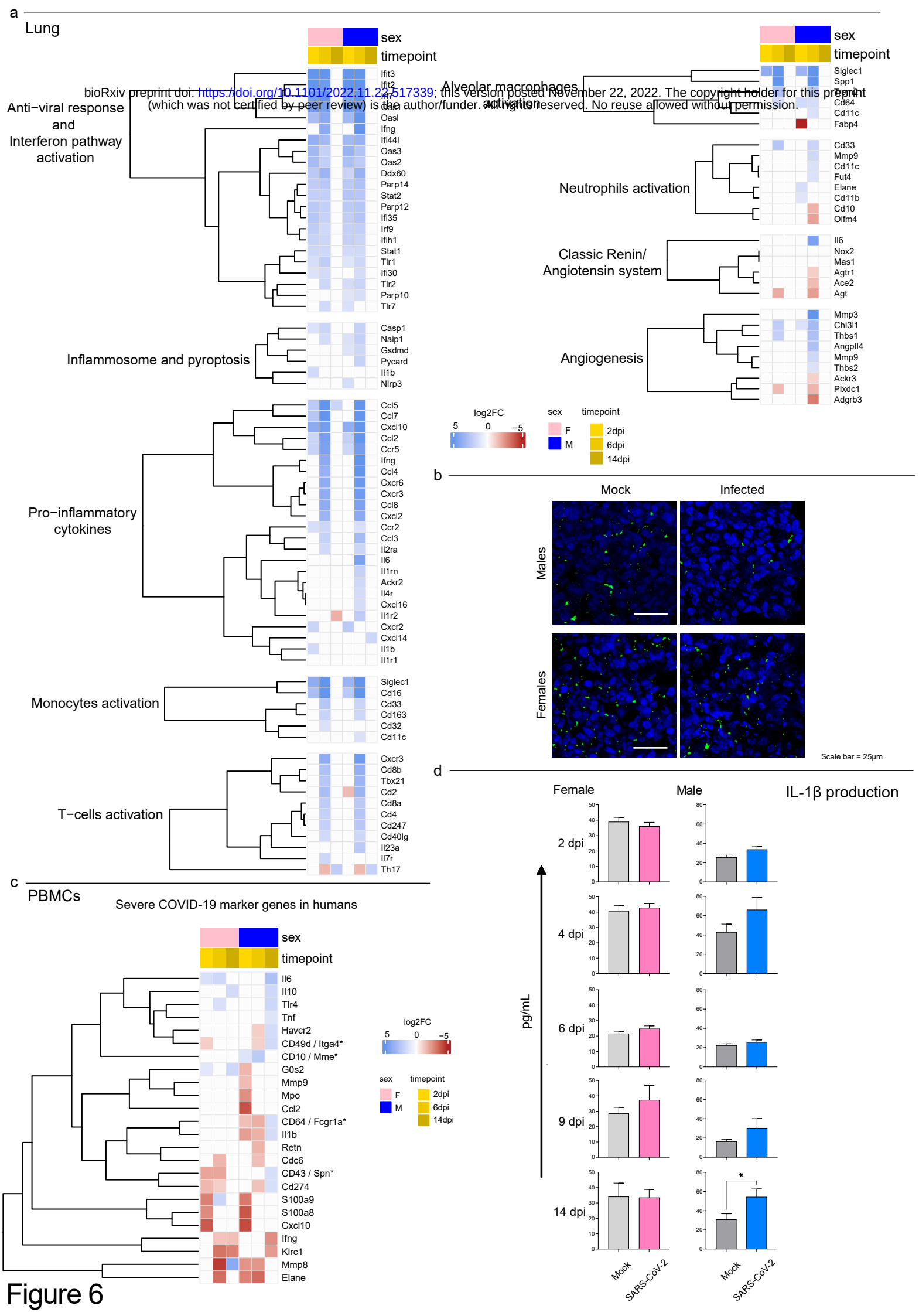

Figure 6